A Stability Result for Periodic Solutions of Nonmonotonic Smooth Negative Feedback Systems

Camille Poignard, Madalena Chaves, Jean-Luc Gouzé

HAL Id: hal-01872255

https://hal.inria.fr/hal-01872255

Submitted on 11 Sep 2018

A Stability Result for Periodic Solutions of Nonmonotonic Smooth Negative Feedback Systems[*]

Camille Poignard[†], Madalena Chaves[‡], and Jean-Luc Gouzé[‡]

Abstract. In high dimension, stability and uniqueness of periodic orbits in nonlinear smooth systems are difficult properties to establish in general. In a previous work, we proved the existence of periodic oscillations inscribed in an invariant torus for a class of negative feedback systems in $\mathbb{R}^n$, where the regulation functions defining these systems are supposed to be nonlinear (and possibly nonmonotonic) in a small window and constant outside this window. Here, under some symmetry assumptions on the parameters of these models, we establish uniqueness and stability of the periodic orbit inside this invariant torus. The method used is based on the analysis of the spectrum of the monodromy matrix associated with the periodic orbit considered. Under the same assumptions, an approximation of the period of the orbit in terms of the parameters is also provided, and all results are illustrated with several examples from circadian rhythms.

Key words. piecewise linear systems, negative feedback circuits, periodic oscillations, monodromy matrix, periodic orbits of vector fields and flows, asymptotic stability, gene regulatory networks

AMS subject classifications. 37C27, 93D20, 92Bxx

DOI. 10.1137/17M1141205

1. Introduction.

Periodic oscillations are often observed in many physical systems, both in natural [9] and in synthetically designed networks [4]. Perhaps the most remarkable periodic phenomena observed in living organisms, circadian rhythms anticipate day/night changes in the environment and prepare the organism to cope with these changes. Circadian rhythms have been detected in a variety of organisms [2] and studied in detail since the 1980s in the fly *Drosophila melanogaster*, the bread mold *Neurospora crassa*, the plant *Arabidopsis thaliana*, and mice, among others. In most cases, the mechanism behind circadian rhythms is a genetic signaling network whose core is a negative feedback loop constituted by a gene (e.g., *period* in fly or *frequency* in *Neurospora* [19]) encoding for a protein which eventually contributes to inhibit its own transcription.

The rapid progress in experimental techniques (e.g., single cell measurements) has opened the way to a wide range of new approaches in the study of biological oscillatory phenomena, and circadian rhythms in particular can be targeted for the development of chronotherapies [5]. It has thus become relevant and useful to develop new mathematical models and theoretical

[†]University of São Paulo, Brazil (camille.poignard@gmail.com).

[‡]Université Côte d'Azur, Inria, INRA, CNRS, UPMC Univ Paris 06, Biocore team, Sophia Antipolis, France (madalena.chaves@inria.fr, jean-luc.gouze@inria.fr).

tools to establish rigorous results on the existence and stability of oscillatory behavior and period computation.

One of the first models to describe negative feedback circuits was suggested by Goodwin in 1965 [10]. This class of models has been studied in detail and exhibits periodic oscillations under some conditions [11]. Goodwin-like models continue to be used to study circadian rhythms as recently as in [19] or [6], where a three-variable negative feedback loop was proposed to represent *Neurospora*'s circadian rhythm. Another well-known contribution to the negative feedback circuit model repertoire is the class of models introduced by L. Glass [8], in a piecewise linear setting, where the regulation functions defining the models are piecewise constant "step" functions (combining piecewise constant production terms with linear degradation terms). More generally, for ordinary differential systems, most of the results found over the last decades required monotonicity assumptions (see [14, 16, 17]) or the use of slow-fast dynamics [7].

Very recently, in [18], we proved the existence of periodic oscillations for a particular class of smooth negative feedback systems in $\mathbb{R}^n$ obtained from piecewise linear ones: More precisely, the regulation functions defining our systems were required to be continuous (or smooth) and equal to the step functions except in a narrow interval $[\theta - \delta, \theta + \delta]$ around the threshold θ of the step function. In this interval $[\theta - \delta, \theta + \delta]$, the nonlinear functions were allowed to be nonmonotonic, which constitutes the main interest of our result presented in [18]. The method we used to prove the existence of periodic oscillations in a model Σ^μ belonging to such a class of systems (where μ denotes the nonlinear regulation function) is to circumscribe Σ^μ by two piecewise linear models Σ^- and Σ^+ and then to prove the existence of two periodic solutions γ^- and γ^+ for these models: These two orbits follow the same cycle $\mathcal{C}$ of regular domains and bound a rectangular torus (i.e., a torus for which each section is a quadrilateral) in which lies a periodic orbit γ^μ for Σ^μ.

The present paper has two objectives: first, to further develop and analyze the stability and uniqueness of the orbit γ^μ and, second, to infer an explicit expression for the period in terms of the system's parameters, based on the stability hypotheses and results. Indeed, here we will prove that, in the particular case where all the degradation terms are equal and under some conditions requiring a symmetry in the dynamic of the model, all periodic orbits of the system Σ^μ following cycle $\mathcal{C}$ are asymptotically stable. In particular, the periodic orbit γ^μ is unique and asymptotically stable in the invariant rectangular torus found in our previous paper [18]. Although the required conditions might appear to be restrictive from a theoretical point of view, our results fit well with data taken from concrete biological situations, as can be seen by the two examples given in section 6 (*Arabidopsis thaliana* and *Neurospora crassa*).

Notice that our result does not guarantee the uniqueness and global stability of γ^μ in the entire phase space of Σ^μ: Outside the torus, other invariant regions can exist with other periodic orbits. Despite this nonglobal unicity, we provide a more accurate localization of the stable periodic orbits. To establish stability, we compute the monodromy matrix for any periodic orbit of Σ_μ: Indeed, the eigenvalues of this matrix determine the stability of the periodic orbit considered [1, 13]. Due to the fact our models are close to piecewise linear ones, the Jacobian of Σ_μ evaluated at a given periodic orbit following cycle $\mathcal{C}$ is triangular in any regular domain of this cycle. We can thus get a complete expression of the monodromy matrix and then perform an estimation of the spectrum of this matrix. This method is an

easier alternative to the computation of the Poincaré map of the section obtained in [18]: Note that the eigenvalues (distinct from the value one) of the Jacobian of this map (i.e., the so-called Floquet exponents) at its fixed point are precisely those of the monodromy matrix.

The rest of the paper is organized as follows. Section 2 defines the smooth negative feedback system Σ^μ introduced and studied in [18]. We define the piecewise linear systems Σ^+ and Σ^- that circumscribe Σ^μ and summarize our previous result on the existence of periodic oscillations for this smooth system. Then, in section 3, we recall the definition of the monodromy matrix for a general differential system and enunciate the stability result linking the spectrum of such a matrix to the stability of its associated periodic orbit. Afterwards, we compute the monodromy matrix of any periodic orbit following cycle $\mathcal{C}$ (see Lemma 3.3). Section 4 states some symmetry conditions on the parameters of the model under which the expression of the monodromy matrix can be simplified: It becomes possible to evaluate the spectrum of this matrix so as to get the main stability result (see Theorem 4.3). Section 5 provides a theoretical approximation for the period and localization of the periodic orbit in terms of the system's parameters. In the symmetrical model case, the period is shown to depend only on the degradation constant and the dimension of the system. Finally, section 6 illustrates our modeling approach by calibrating our model to data from *Arabidopsis* and *Neurospora* circadian rhythms.

2. The smooth negative feedback system Σ^μ. As explained in the introduction, the smooth model Σ^μ introduced in [18] is a differential system coming from piecewise linear systems of the form

$$(\mathcal{S}) \begin{cases} \dot{x_1} & = \kappa_1(x) - \gamma_1 x_1 \\ & \vdots \\ \dot{x_n} & = \kappa_n(x) - \gamma_n x_n, \end{cases}$$

in which all γ_i are positive real numbers, each variable x_i is in $\mathbb{R}_+^n$, and each function $\kappa_i : \mathbb{R}_+^n \to \mathbb{R}_+$ is a sum of products of functions of the form $s^+(\cdot, \theta)$ and $s^-(\cdot, \theta)$, where $s^+(\cdot, \theta)$ is the classical step function with threshold θ,

$$\begin{cases} s^+(z, \theta) & := 0 \text{ if } z < \theta \\ s^+(z, \theta) & := 1 \text{ if } z > \theta, \end{cases}$$

and $s^-(\cdot, \theta)$ is defined by the relation $s^-(\cdot, \theta) := 1 - s^+(\cdot, \theta)$. We recall that the dynamics of such a system $(\mathcal{S})$ evolves in a rectangular region of $\mathbb{R}_+^n$ that can be decomposed in rectangular *regular domains* (also called "boxes") and *switching domains* (or the boundaries between regular domains): In a given regular domain B, the flow converges to a unique fixed point denoted by $(k_1(B)/\gamma_1, \ldots, k_n(B)/\gamma_n)$, where $k_i(B)$ stands for the constant value of κ_i in the box B.

As in [18], we will only consider the case where each focal point of a regular domain B is outside B in order to prevent having a trivial asymptotic stationary dynamics in a box. **We will also consider the case where all switching domains are transparent**, i.e., where the trajectories can be extended continuously in the switching domains, avoiding by the way singular cases (see, for instance, [3]). We refer the reader to section 2.2 of our previous paper
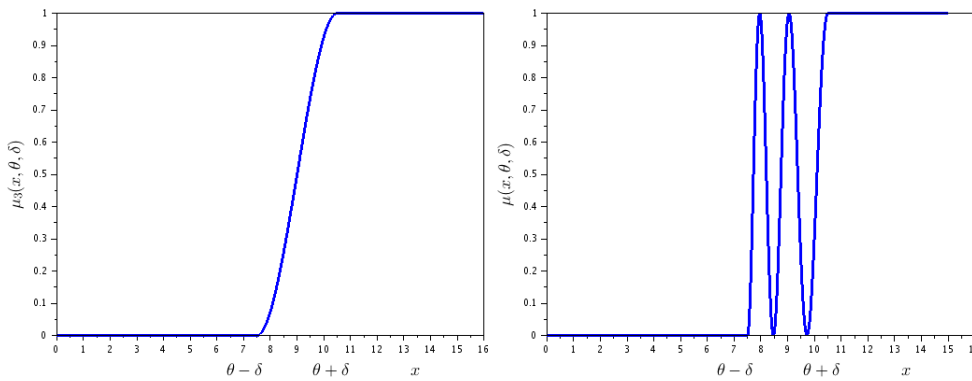
Figure 1. *Two examples of function μ: monotonic or sinusoidal.*

[18] for more details about these basic facts on the piecewise linear setting or to [8] for a more complete introduction on this subject.

2.1. Definition of the negative feedback system $\Sigma_{\theta,k,\gamma,\delta}^{\mu}$. The underlying system is a negative feedback loop, a motif which frequently appears in biological networks [4, 20]. A corresponding piecewise linear model $\Sigma_{\theta,k,\gamma,\delta}$ can be written as

$$\Sigma_{\theta,k,\gamma} : \begin{cases} \dot{x_1} &= k_1 s^- \left(x_3, \theta_3 \right) - \gamma_1 x_1 \\ &\vdots \\ \dot{x_i} &= k_i s^+ \left(x_{i-1}, \theta_{i-1} \right) - \gamma_i x_i, \quad i = 2, \ldots, n. \end{cases}$$

Now, given a real number $\delta > 0$, the system $\Sigma_{\theta,k,\gamma,\delta}^{\mu}$ we have studied in [18] is a smooth version of $\Sigma_{\theta,k,\gamma}$,

$$\Sigma_{\theta,k,\gamma,\delta}^{\mu} : \begin{cases} \dot{x_1} &= k_1 \mu^- \left(x_3, \theta_3, \delta \right) - \gamma_1 x_1 \\ &\vdots \\ \dot{x_i} &= k_i \mu^+ \left(x_{i-1}, \theta_{i-1}, \delta \right) - \gamma_i x_i, \quad i = 2, \ldots, \end{cases}$$

in which the functions $\mu^-(\cdot, \theta, \delta) : \mathbb{R}_+ \to [0, 1]$ and $\mu^+(\cdot, \theta, \delta) : \mathbb{R}_+ \to [0, 1]$ are continuous or smooth functions coinciding with $s^-(\cdot, \theta)$ and $s^+(\cdot, \theta)$, except in a narrow window of size 2δ around the threshold θ, where they can be monotonic or not, i.e.,

$$\mu^+ (x, \theta_i, \delta) := \begin{cases} 0 & \text{if } x \leq \theta_i - \delta \\ \overline{\mu^+} (x, \theta_i, \delta) & \text{if } \theta_i - \delta \leq x \leq \theta_i + \delta \\ 1, & \text{if } \theta_i + \delta \leq x, \end{cases}$$

where $\overline{\mu^+}$ is at least $\mathcal{C}^1$ and satisfies $\overline{\mu^+}(\theta_i - \delta, \theta_i, \delta) = 0$ and $\overline{\mu^+}(\theta_i + \delta, \theta_i, \delta) = 1$ (see Figure 1). Similarly for μ^-.

Thus, by defining $\Sigma_{\theta,k,\gamma,\delta}^{\mu}$ in this way, we have transformed the piecewise linear system $\Sigma_{\theta,k,\gamma}$ into a smooth one by layering, in the phase space, regular domains between the domains associated to $\Sigma_{\theta,k,\gamma}$, namely, the domains of the form $\{x \in \mathbb{R}_+^n : \exists i \in \{1, \ldots, n\} : \theta_i - \delta < x_i <$

$\theta_i + \delta$}. Therefore, the rectangular region $[0, \dfrac{k_1}{\gamma_1}] \times \cdots \times [0, \dfrac{k_n}{\gamma_n}]$ is going to be decomposed into 3^n boxes depending on whether the ith coordinate x_i of a point x is below $\theta_i - \delta$, belongs to $[\theta_i - \delta, \theta_i + \delta]$, or is above $\theta_i + \delta$.

2.2. The exterior system $\Sigma^+_{\theta,k,\gamma,\delta}$ and the interior system $\Sigma^-_{\theta,k,\gamma,\delta}$. The existence of periodic oscillations for $\Sigma^\mu_{\theta,k,\gamma,\delta}$ relies on the bounding of this system by two piecewise linear systems. These are constructed from the step function $s^+(\cdot, \theta_i - \delta)$ bounding $\mu_i{}^+$ from above and $s^+(\cdot, \theta_i + \delta)$ bounding $\mu_i{}^+$ from below (see Figure 1) and similarly for $\mu_i{}^-$ bounded by the step functions $s^-(\cdot, \theta_i - \delta)$ and $s^-(\cdot, \theta_i + \delta)$. More precisely, these systems are the exterior system denoted by $\Sigma^+_{\theta,k,\gamma,\delta}$,

$$\Sigma^+_{\theta,k,\gamma,\delta} : \begin{cases} \dot{x}_1(t) = k_1 \left(s^-(x_3, \theta_3 + \delta) s^+(x_1, \theta_1 + \delta) + s^-(x_3, \theta_3 - \delta) s^-(x_1, \theta_1 + \delta) \right) - \gamma_1 x_1 \\ \vdots \\ \dot{x}_i(t) = k_i \left(s^+(x_{i-1}, \theta_{i-1} + \delta) s^-(x_i, \theta_i + \delta) + s^+(x_{i-1}, \theta_{i-1} - \delta) s^+(x_i, \theta_i + \delta) \right) - \gamma_i x_i, \end{cases}$$

and the interior system denoted by $\Sigma^-_{\theta,k,\gamma,\delta}$,

$$\Sigma^-_{\theta,k,\gamma,\delta} : \begin{cases} \dot{x}_1(t) = k_1 \left(s^-(x_3, \theta_3 - \delta) s^+(x_1, \theta_1 + \delta) + s^-(x_3, \theta_3 + \delta) s^-(x_1, \theta_1 + \delta) \right) - \gamma_1 x_1 \\ \vdots \\ \dot{x}_i(t) = k_i \left(s^+(x_{i-1}, \theta_{i-1} - \delta) s^-(x_i, \theta_i + \delta) + s^+(x_{i-1}, \theta_{i-1} + \delta) s^+(x_i, \theta_i + \delta) \right) - \gamma_i x_i, \end{cases}$$

for $i = 2, \ldots, n$. The idea to obtain these equations is illustrated by Figure 2: We consider extended versions of the original model $\Sigma_{\theta,k,\gamma}$ when each threshold θ_i is replaced by the two thresholds $\theta_i - \delta$ and $\theta_i + \delta$. Each time we reach a switching domain defined by $\theta_i - \delta$, we can either switch directly to the dynamics defined by another vector field (first possibility) or continue with the same dynamics until we reach the switching domain defined by the threshold $\theta_i + \delta$ (second possibility). Our two piecewise linear models $\Sigma^-_{\theta,k,\gamma,\delta}$ and $\Sigma^+_{\theta,k,\gamma,\delta}$ are built precisely according to these two possibilities.

As said above, we now have 3^n regular domains for the dynamics of $\Sigma^+_{\theta,k,\gamma,\delta}$, $\Sigma^-_{\theta,k,\gamma,\delta}$ (and thus for $\Sigma^\mu_{\theta,k,\gamma,\delta}$ as well).

Notation 2.1. *Let $B_{a_1 \cdots a_n}$ denote each of the 3^n regular domains associated to the systems $\Sigma^+_{\theta,k,\gamma,\delta}$ and $\Sigma^-_{\theta,k,\gamma,\delta}$, where the tuples $(a_1, \ldots, a_n)$ belong to $\{0, 1, 2\}^n$ and are defined by*

$$\forall\, 1 \leq i \leq n, \ a_i = \begin{cases} 0 & \text{if } 0 < x_i < \theta_i - \delta \\ 1 & \text{if } \theta_i - \delta < x_i < \theta_i + \delta \\ 2 & \text{if } \theta_i + \delta < x_i. \end{cases}$$

2.3. Existence of periodic orbits for the system $\Sigma^\mu_{\theta,k,\gamma,\delta}$. The result proved in [18] can now be summarized.

Notation 2.2. *Let $\phi^-_t, \phi^+_t, \phi^\mu_t$ denote the three flows of the systems $\Sigma^-_{\theta,k,\gamma,\delta}, \Sigma^+_{\theta,k,\gamma,\delta}, \Sigma^\mu_{\theta,k,\gamma,\delta}$.*

It was shown in [18] that, under some assumptions, $\Sigma^-_{\theta,k,\gamma,\delta}$ admits a periodic orbit $(\phi^-_s(z^-))_{s \in \mathbb{R}}$ and $\Sigma^+_{\theta,k,\gamma,\delta}$ a periodic orbit $(\phi^+_s(z^+))_{s \in \mathbb{R}}$, where the two points z^- and z^+ were
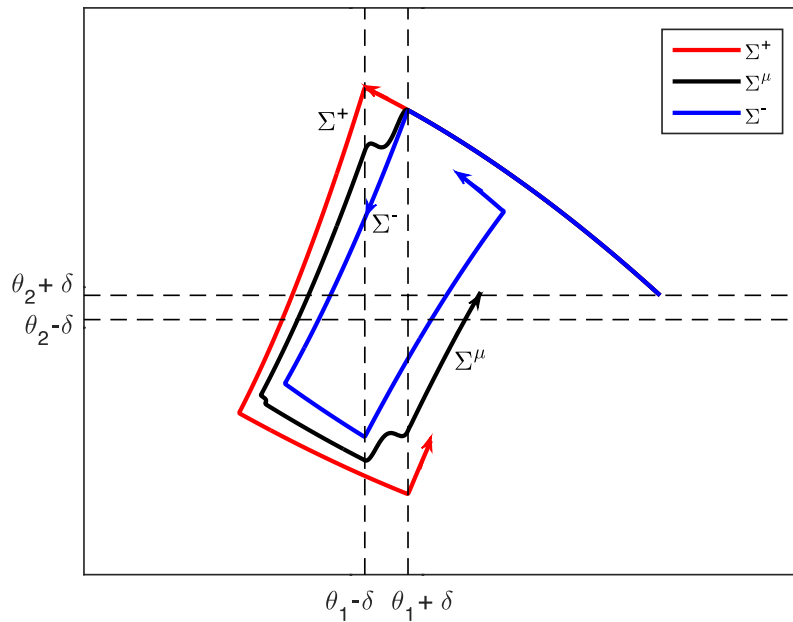
Figure 2. *Constructing the exterior and interior piecewise linear systems. The trajectories of Σ^+, Σ^-, and Σ^μ are projected in the plane x_1, x_2.*

chosen in the switching domain $B_{222\cdots2} \cap \{x_1 = \theta_1 + \delta\}$. These two orbits follow cycle $\mathcal{C}$ defined by

$$\mathcal{C}: \begin{array}{ccccccccc} B_{222\cdots2} & \rightarrow & B_{122\cdots2} & \rightarrow & B_{022\cdots2} & \rightarrow & B_{012\cdots2} & \rightarrow & \cdots \rightarrow B_{00\cdots01} \\ \uparrow & & & & & & & & \downarrow \\ B_{22\cdots21} & \leftarrow & \cdots \leftarrow & B_{210\cdots0} & \leftarrow & B_{200\cdots0} & \leftarrow & B_{100\cdots0} & \leftarrow & B_{000\cdots0}. \end{array}$$

Then, for any x taken in a given rectangular section delimited by z^- and z^+ and for any time t, the point $\phi_t^\mu(x)$ satisfies the relation $\phi_t^\mu(x)_i \in [\phi_t^-(z^-)_i, \phi_t^+(z^+)_i] \cup [\phi_t^+(z^+)_i, \phi_t^-(z^-)_i]$ for any $1 \leq i \leq n$.

In this way, we have shown that there exists a Poincaré section for the system $\Sigma_{\theta,k,\gamma,\delta}^\mu$ (at a fixed distance independent on δ from the point $(\theta_1, \ldots, \theta_n)$) and thus a periodic orbit for this system.

Theorem 2.3. *Given a real number $\eta > 0$, assume that the following hypotheses on the parameters $(k_i, \gamma_i, \theta_i)_{1 \leq i \leq n}$ and δ are satisfied: For every $1 \leq i \leq n$, $\theta_i > 0$, and for every $2 \leq i \leq n$, $\dfrac{k_i}{\gamma_i} > \theta_i + \eta$.*

Then there exists a number $\Lambda_0 > \eta$ and a number δ_0 satisfying $0 < \delta_0 < \min_{1 \leq i \leq n} \left(\theta_i, \dfrac{k_i}{\gamma_i} - \theta_i, 1\right)$ such that for every $\dfrac{k_1}{\gamma_1} > \Lambda_0 + \theta_1$ and every $0 < \delta \leq \delta_0$, the continuous system $\Sigma_{\theta,k,\gamma,\delta}^\mu$ admits a periodic orbit γ^μ following cycle $\mathcal{C}$.

In fact, numerical simulations we have performed have shown that for small values of δ, the system $\Sigma_{\theta,k,\gamma,\delta}^\mu$ can have a fixed point in the cube $\mathcal{C}_\delta = [\theta_1 - \delta, \theta_1 + \delta] \times [\theta_2 - \delta, \theta_2 + \delta] \times \cdots \times$

$[\theta_n - \delta, \theta_n + \delta]$ around the point $(\theta_1, \ldots, \theta_n)$: Therefore, the introduction of the parameter η in the assumptions of this result is made precisely to ensure the existence of a Poincaré section at a distance η from this center point (see Figure 8 in section 6 for an example).

In this paper, we establish stability and uniqueness of this orbit γ^μ. To do this, we use, in the next section, an approach based on the monodromy matrix [1, 13] associated to any given periodic orbit. Some properties on the eigenvalues of the monodromy matrix ensure stability of the orbit (see Proposition 3.1 below), and then Lefschetz Fixed-Point Theory implies uniqueness of the orbit.

Notation 2.4. *In the rest of the paper, the following notation will be used:*

$$\mu_n^- = \mu^- \left(\cdot, \theta_n, \delta \right)$$
$$\mu_i^+ = \mu^+ \left(\cdot, \theta_i, \delta \right), \quad i = 1, \ldots, n - 1.$$

Notation 2.5. *In the rest of the text, F_μ denotes the vector field defining the system $\Sigma_{\theta, k, \gamma, \delta}^\mu$.*

3. The monodromy matrix of the system $\Sigma_{\theta, k, \gamma, \delta}^\mu$.

3.1. Review of monodromy matrices. Our approach is based on the computation of a monodromy matrix for the differential system $\Sigma_{\theta, k, \gamma, \delta}^\mu$: First, recall the basic proposition relating the stability of a periodic orbit to its monodromy matrix. We refer the reader interested in this topic to [1] for a complete introduction (that is not needed here) on this subject.

Generally speaking, given a differential system $\dot{x} = F(x, p)$ in $\mathbb{R}^n$ depending on a family of parameters p and admitting a periodic orbit $x^*(t)$, let us consider the following matrix differential system:

(1)
$$\begin{cases} \dot{Z}(t) = \dfrac{\partial F\left(x^*(t), p\right)}{\partial x} Z(t) \\ Z(0) = I_n, \end{cases}$$

where I_n stands for the identity matrix in $\mathbb{R}^n$. Then *the monodromy matrix* of the vector field $F(\cdot, p)$ associated to the periodic orbit $x^*(t)$ is the matrix $Z(T^*)$ solution of this differential system taken at the time T^*, where T^* is the period of $x^*(t)$. The interest of this particular matrix lies in the following result [1, 13].

Proposition 3.1. *Let $\mathfrak{S}(Z(T^*))$ be the spectrum of the monodromy matrix $Z(T^*)$ of the system $\dot{x} = F(x, p)$ associated to the periodic orbit $x^*(t)$. Then*
  1. *the value 1 belongs to $\mathfrak{S}(Z(T^*))$;*
  2. *if for every eigenvalue $\lambda \in \mathfrak{S}(Z(T^*)) \setminus 1$ we have $|\lambda| < 1$, then $x^*(t)$ is asymptotically stable;*
  3. *if there exists an eigenvalue $\lambda \in \mathfrak{S}(Z(T^*)) \setminus 1$ such that $|\lambda| > 1$, then $x^*(t)$ is unstable.*

3.2. Computation of the monodromy matrix of $\Sigma_{\theta, k, \gamma, \delta}^\mu$. Considering now the vector field F_μ, we know it admits a periodic orbit (Theorem 2.3 and [18]). Our goal is to compute the monodromy matrix associated to such an orbit and study its spectrum. To do this, consider now any periodic orbit $x^*(t)$ of F_μ of the n-dimensional system, and assume (without loss of generality) it starts at an initial condition $x^*(0)$ belonging to the switching domain $B_{22\ldots2} \cap \{x_n = \theta_n + \delta\}$.

This periodic orbit crosses the $4n$ regular domains $B_{a_1 a_2 \cdots a_n}$ of cycle $\mathcal{C}$. The times spent in each of them can be divided into two categories: the times s_i^d and s_i^c (for $1 \leq i \leq n$) corresponding to the times spent in a box $B_{a_1 a_2 \cdots a_n}$ with $a_i = 1$ and the times t_i^d and t_i^c spent in a box $B_{a_1 a_2 \cdots a_n}$ with all $a_i \neq 1$:

(2)

$$
\begin{array}{ccccccccc}
& t_1^d & & s_1^d & & t_2^d & & s_2^d & & s_n^d \\
x^*(0) \in B_{222\cdots 2} & \rightarrow & B_{122\cdots 2} & \rightarrow & B_{022\cdots 2} & \rightarrow & B_{012\cdots 2} & \rightarrow & \cdots & \rightarrow B_{00\cdots 01} \\
\uparrow & & & & & & & & \downarrow \\
B_{22\cdots 21} & \leftarrow & \cdots \leftarrow & B_{210\cdots 0} & \leftarrow & B_{200\cdots 0} & \leftarrow & B_{100\cdots 0} & \leftarrow & B_{000\cdots 0} \\
s_n^c & & & s_2^c & & t_2^c & & s_1^c & & t_1^c.
\end{array}
$$

In these notations, the letter "d" stands for "decreasing" and corresponds to the case where the coordinate i is decreasing when the periodic orbit is crossing the box considered, and the same for "c," which stands for "increasing." These values are used to compute the time necessary to reach each box of $\mathcal{C}$ starting from $x^*(0)$.

Notation 3.2. *For $x^*(t)$, a periodic orbit of $\Sigma_{\theta,k,\gamma,\delta}^\mu$ following cycle $\mathcal{C}$ with $x^*(0)$ in $B_{22\cdots 2} \cap \{x_n = \theta_n + \delta\}$, denote by $(T_i)_{i=1,\ldots,4n}$ the family of intermediate times necessary for $x^*(t)$ to reach the ith box from $x^*(0)$ (see (2)), before returning to $B_{22\cdots 2} \cap \{x_n = \theta_n + \delta\}$:*

$$
\begin{cases}
T_1 & = t_1^d \\
T_2 & = t_1^d + s_1^d \\
T_3 & = t_1^d + s_1^d + t_2^d \\
\vdots \\
T_{2n} & = \sum_{i=1}^n \left(t_i^d + s_i^d \right) \\
T_{2n+1} & = \sum_{i=1}^n \left(t_i^d + s_i^d \right) + t_1^c \\
\vdots \\
T_{4n} & = \sum_{i=1}^n \left(t_i^d + s_i^d \right) + \sum_{i=1}^n \left(t_i^c + s_i^c \right).
\end{cases}
$$

Under this notation, the period of the orbit $x^*(t)$ is T_{4n}. Now we have the following:

Lemma 3.3. *Let $x^*(t)$ be a periodic orbit of $\Sigma_{\theta,k,\gamma,\delta}^\mu$ following cycle $\mathcal{C}$ with $x^*(0)$ belonging to $B_{22\cdots 2} \cap \{x_n = \theta_n + \delta\}$ and $(T_i)_{i=1,\ldots,4n}$ be the family of intermediate times associated to $x^*(t)$. Then the monodromy matrix $Z(T_{4n})$ of $x^*(t)$ is equal to*

$$Z(T_{4n}) = U(c_1, T_{4n} - T_{4n-1}) \, W(c_2, \ldots, c_n, T_{4n-1} - T_{2n}) \, U(\tilde{c}_1, T_{2n} - T_{2n-1}) \, W(\tilde{c}_2, \ldots, \tilde{c}_n, T_{2n}),$$

where the matrices U are upper triangular and W lower triangular, defined by

$$
U(r_1, \tau) =
\begin{bmatrix}
e^{-\gamma_1 \tau} & 0 & 0 & \cdots & 0 & r_1 \\
0 & e^{-\gamma_2 \tau} & 0 & \cdots & 0 & 0 \\
\vdots & \vdots & \vdots & & \vdots & \vdots \\
0 & 0 & 0 & \cdots & 0 & e^{-\gamma_n \tau}
\end{bmatrix}
$$

and

$$W(r_2,\ldots,r_n,\tau) = \begin{bmatrix} e^{-\gamma_1\tau} & 0 & 0 & 0 & 0 & \cdots & 0 & 0 \\[2mm] r_2 & e^{-\gamma_2\tau} & 0 & 0 & 0 & \cdots & 0 & 0 \\[2mm] r_2 r_3 & r_3 & e^{-\gamma_3\tau} & 0 & 0 & \cdots & 0 & 0 \\[2mm] r_2 r_3 r_4 & r_3 r_4 & r_4 & e^{-\gamma_4\tau} & 0 & \cdots & 0 & 0 \\[2mm] \vdots & \vdots & \vdots & \vdots & \vdots & & \vdots & \vdots \\[2mm] r_2\cdots r_n & r_3\cdots r_n & r_4\cdots r_n & \cdots & \cdots & \cdots & r_n & e^{-\gamma_n\tau} \end{bmatrix},$$

and the constants $(c_i,\tilde{c}_i)_{i=1,\ldots,n}$ *equal*

$$c_1 = k_1 e^{-\gamma_1 T_{4n}+\gamma_n T_{4n-1}} \int_{T_{4n-1}}^{T_{4n}} {\mu_n^{-}}'\left(x_n^*(s)\right) e^{(\gamma_1-\gamma_n)s}ds$$

$$c_i = k_i e^{-\gamma_i T_{4n}+\gamma_{i-1}T_{4n-1}} \int_{T_{2n+2(i-1)-1}}^{T_{2n+2(i-1)}} {\mu_{i-1}^{+}}'\left(x_{i-1}^*(s)\right) e^{(\gamma_i-\gamma_{i-1})s}ds, \quad i=2,\ldots,n$$

$$\tilde{c}_1 = k_1 e^{-\gamma_1 T_{2n}+\gamma_n T_{2n-1}} \int_{T_{2n-1}}^{T_{2n}} {\mu_n^{-}}'\left(x_n^*(s)\right) e^{(\gamma_1-\gamma_n)s}ds$$

$$\tilde{c}_i = k_i e^{-\gamma_i T_{2n-1}} \int_{T_{2(i-1)-1}}^{T_{2(i-1)}} {\mu_{i-1}^{+}}'\left(x_{i-1}^*(s)\right) e^{(\gamma_i-\gamma_{i-1})s}ds, \quad i=2,\ldots,n.$$

Proof. Let $x^*(t)$ be a periodic orbit. We have, for any time t,

$$\frac{\partial F_\mu}{\partial x}\left(x^*(t)\right) = \begin{bmatrix} -\gamma_1 & 0 & 0 & \cdots & 0 & 0 & k_1 {\mu_n^{-}}'\left(x_n^*(t)\right) \\[2mm] k_2 {\mu_1^{+}}'\left(x_1^*(t)\right) & -\gamma_2 & 0 & \cdots & 0 & 0 & 0 \\ \vdots & \vdots & \vdots & & \vdots & \vdots & \vdots \\[2mm] 0 & 0 & 0 & \cdots & 0 & k_n {\mu_{n-1}^{+}}'\left(x_{n-1}^*(t)\right) & -\gamma_n \end{bmatrix},$$

and note that, at each box in cycle $\mathcal{C}$, at most one of the off-diagonal components is nonzero: Only the variable x_i with index i equal to one is in the region $\theta_i - \delta < x_i^*(t) < \theta_i + \delta$, where μ_i is not constant.

In addition, notice that the matrix $\frac{\partial F_\mu}{\partial x}(x^*(t))$ is either diagonal (in the boxes whose label contains no "1"), upper triangular in the boxes $B_{00\cdots01}$ and $B_{22\cdots21}$ (corresponding, respectively, to the time intervals $[T_{2n-1}, T_{2n}]$, $[T_{4n-1}, T_{4n}]$), or lower triangular in any other regular domain.

Following these observations, the matrix $Z(T^*)$ can be computed iteratively in four parts.

(i) First consider the restriction of the matrix equation (1) (taken with $F = F_\mu$) to the interval $[T_{4n-1}, T_{4n})$, which corresponds to the trajectory $x^*(t)$ restricted to the regular domain $B_{22\cdots21}$, where for all t in (T_{4n-1}, T_{4n})

$$\forall i \in \{1, \ldots, n-1\}: \ x_i^*(t) > \theta_i + \delta$$
$$\theta_n - \delta < x_n^*(t) < \theta_n + \delta,$$

and so only the off-diagonal term $k_1 \mu_n^{-\prime}(x_n^*(t))$ is nonzero. Thus, (1) (taken with $F = F_\mu$) restricted to $[T_{4n-1}, T_{4n}]$ is a triangular matrix system, for which solution $Z(t)$ can be fully expressed step-by-step. Integrating this system, we get, for any time t in $[T_{4n-1}, T_{4n}]$,

$$Z(T_{4n}) = U(c_1, T_{4n} - T_{4n-1})Z(T_{4n-1}).$$

(ii) Now let us compute $Z(T_{4n-1})$. Note that in the interval (T_{4n-2}, T_{4n-1}), the orbit crosses the box $B_{2\cdots 220}$, where the monodromy matrix is diagonal,

$$\frac{\partial F_\mu}{\partial x}(x^*(t)) = \ \text{diag}(-\gamma_1, -\gamma_2, \ldots, -\gamma_n),$$

so that a simple integration gives

$$Z(T_{4n-1}) = \text{diag}(-\gamma_1(T_{4n-1}-T_{4n-2}), -\gamma_2(T_{4n-1}-T_{4n-2}), \ldots, -\gamma_n(T_{4n-1}-T_{4n-2}))\, Z(T_{4n-2}).$$

In contrast, in the interval (T_{4n-3}, T_{4n-2}), the orbit crosses the box $B_{2\cdots 210}$, where the matrix $\frac{\partial F_\mu}{\partial x}(x^*(t))$ is lower triangular:

$$\frac{\partial F_\mu}{\partial x}(x^*(t)) = \begin{bmatrix} -\gamma_1 & 0 & 0 & \cdots & 0 & 0 & 0 \\ 0 & -\gamma_2 & 0 & \cdots & 0 & 0 & 0 \\ \vdots & \vdots & \vdots & & \vdots & \vdots & \vdots \\ 0 & 0 & 0 & \cdots & 0 & -\gamma_{n-1} & 0 \\ 0 & 0 & 0 & \cdots & 0 & k_n \mu_{n-1}^{+\prime}\left(x_{n-1}^*(t)\right) & -\gamma_n \end{bmatrix}.$$

Combining these two steps, we obtain, for the interval (T_{4n-3}, T_{4n-1}),

$$Z(T_{4n-1}) = \begin{bmatrix} e^{-\gamma_1(T_{4n-1}-T_{4n-3})} & 0 & 0 & \cdots & 0 & 0 & 0 \\ 0 & e^{-\gamma_2(T_{4n-1}-T_{4n-3})} & 0 & \cdots & 0 & 0 & 0 \\ \vdots & \vdots & \vdots & \vdots & \vdots & & \vdots \\ 0 & 0 & 0 & \cdots & 0 & z_{n,n-1} & e^{-\gamma_n(T_{4n-1}-T_{4n-3})} \end{bmatrix}$$
$$Z(T_{4n-3}),$$

where

$$z_{n,n-1} = k_n e^{-\gamma_n T_{4n-2}+\gamma_{n-1}T_{4n-3}} \int_{T_{4n-3}}^{T_{4n-2}} \mu_{n-1}^{+\prime}(x_{n-1}^*(t)) e^{\gamma_n - \gamma_{n-1}} ds.$$

If we write $Z(T_{4n-1}) = Q_n Z(T_{4n-3})$, it is now easy to generalize the integration for the remaining boxes down to $B_{10\cdots0}$:

$$Z(T_{4n-1}) = Q_n \cdots Q_3 Q_2 Z(T_{2n}) = W(c_2, \ldots, c_n, T_{4n-1} - T_{2n}) \, Z(T_{2n}). \qquad \blacksquare$$

(iii) Similary to part (i), the step $Z(T_{2n}) = U(\tilde{c}_1, T_{2n} - T_{2n-1})Z(T_{2n-1})$ is also given by an upper triangular matrix.

(iv) For the remaining iterations, the Jacobian matrix is always lower triangular, and the calculations are similar to part (ii), $Z(T_{2n-1}) = W(\tilde{c}_2, \ldots, \tilde{c}_n, T_{2n-1} - T_0)Z(T_0)$, where $T_0 = 0$.

All together, (i)–(iv) yield the desired result.

4. A result on the stability of periodic orbits for $\Sigma^\mu_{\theta,k,\gamma,\delta}$. Lemma 3.3 gives a general expression of the monodromy matrix $Z(T_{4n})$. As said above, stability of the periodic orbit $x^*(t)$ can be obtained by analyzing the spectrum $\mathfrak{S}(Z(T_{4n}))$. However, in general, it is not possible to compute directly the eigenvalues of $Z(T_{4n})$ or to evaluate them; to do this, we need to add further assumptions (see hypotheses **H1** and **H2** below and hypothesis **H3** (used in Theorem 4.3), under which the expression of $Z(T_{4n})$ takes a much more simple form:

H1: The parameters $\gamma_i = \gamma$ are all equal.

H2: All the ratios k_i/γ_i satisfy $k_i/\gamma_i = 2\theta_i$ with $k_1/\gamma_1 > \Lambda_0$ and $\delta < \delta_0$ (where Λ_0, δ_0 are the constants of Theorem 2.3).

H3: $\forall i \in \{1, \ldots, n\}: \ c_i = \tilde{c}_i$ and

$$G := e^{-\gamma T_{4n}/2} < \frac{1}{n-1}.$$

These hypotheses require some symmetries in the model $\Sigma^\mu_{\theta,k,\gamma,\delta}$: **H1** states that all degradation rates are equal, which simplifies the form of the explicit solutions in each box; **H2** states that the threshold θ_i corresponds exactly to the middle of the (invariant) interval $[0, k_i/\gamma_i]$ for all i; and, finally, $c_i = \tilde{c}_i$ in **H3** corresponds to saying that crossing the "first half" of cycle $\mathcal{C}$ (i.e., from the box $B_{22\cdots2}$ to $B_{00\cdots01}$) of the periodic orbit has the same effect as crossing the other half of $\mathcal{C}$ (i.e., from $B_{00\cdots0}$ to $B_{22\cdots21}$); that is, the monodromy matrix can be written as a square. It should be remarked that although these hypotheses introduce some restrictions on the parameters, they still include many relevant cases, as illustrated by several examples in sections 5 and 6.

To get our stability result (Theorem 4.3 below), the first thing we need to verify is that Assumptions **H1**, **H2**, and **H3** are consistent with the hypotheses of Theorem 2.3 required to ensure the existence of a periodic orbit for $\Sigma^\mu_{\theta,k,\gamma,\delta}$.

Lemma 4.1. *Assume the vector field F_μ of $\Sigma^\mu_{\theta,k,\gamma,\delta}$ satisfies **H1** and **H2**. Then the system $\Sigma^\mu_{\theta,k,\gamma,\delta}$ admits a periodic orbit following cycle $\mathcal{C}$.*

Proof. It suffices to apply Theorem 2.3 with $\eta = \dfrac{1}{2}\min(\theta_2, \ldots, \theta_n)$ with $\theta_1 > \Lambda_0$ and with $\delta < \delta_0$. $\blacksquare$

Lemma 4.2. *Assume the vector field F_μ of $\Sigma^\mu_{\theta,k,\gamma,\delta}$ satisfies the assumptions **H1** and **H2**. Let $x^*(t)$ be a periodic orbit of $\Sigma^\mu_{\theta,k,\gamma,\delta}$ following cycle $\mathcal{C}$ with $x^*(0)$ belonging to $B_{22\cdots2} \cap \{x_n = $*

$\theta_n + \delta\}$, and let T_{4n} the period of $x^*(t)$. Then the monodromy matrix $Z(T_{4n})$ associated to $x^*(t)$ is equal to

$$Z(T_{4n}) = e^{-\gamma T_{4n}} U(c_1, 0) \, W(c_2, \ldots, c_n, 0) \, U(\tilde{c}_1, 0) \, W(\tilde{c}_2, \ldots, \tilde{c}_n, 0),$$

and the constants $(c_i, \tilde{c}_i)_{i=1,\ldots,n}$ in Lemma 3.3 are equal to

$$c_1 = \frac{k_1}{\gamma_1} \int_{\theta_n - \delta}^{\theta_n + \delta} \frac{\mu_n^{-'}(u)}{2\theta_n - u} du$$

$$c_i = \frac{k_i}{\gamma_i} \int_{\theta_{i-1} - \delta}^{\theta_{i-1} + \delta} \frac{\mu_{i-1}^{+'}(u)}{2\theta_{i-1} - u} du, \quad i = 2, \ldots, n$$

$$\tilde{c}_1 = \frac{k_1}{\gamma_1} \int_{\theta_n - \delta}^{\theta_n + \delta} \frac{\mu_n^{-'}(u)}{u} du$$

$$\tilde{c}_i = \frac{k_i}{\gamma_i} \int_{\theta_{i-1} - \delta}^{\theta_{i-1} + \delta} \frac{\mu_{i-1}^{+'}(u)}{u} du, \quad i = 2, \ldots, n.$$

Proof. Consider again the matrix $Z(T_{4n})$ obtained in Lemma 3.3. Under **H1**, all degradation rates are equal, so all the exponential terms in the matrices U and W can be factored out and simplified in a straightforward way to yield the term $e^{-\gamma T_{4n}}$.

To compute the coefficients $(c_i)_{i=1,\ldots,n}$ and $(\tilde{c}_i)_{i=1,\ldots,n}$, consider c_1. Between T_{4n-1} and T_{4n}, the orbit $x^*(t)$ crosses the box $B_{22\ldots21}$, and in this box the flows ϕ_t^+ and ϕ_t^- of the exterior and interior systems $\Sigma_{\theta,k,\gamma,\delta}^+$ and $\Sigma_{\theta,k,\gamma,\delta}^-$ surrounding the smooth system $\Sigma_{\theta,k,\gamma,\delta}^\mu$ (see [18]) satisfy the relation

$$\left(\phi_t^+(x)\right)_n = \left(\phi_t^-(x)\right)_n.$$

Thus, we have

$$\forall s \in [T_{4n-1}, T_{4n}]: \ x_n^*(s) = \frac{k_n}{\gamma} + e^{-\gamma s}\left(x_n(T_{4n-1}) - s\right).$$

Then, by making the change of variable,

$$\begin{cases} u &= x_n^*(s) \\ du &= x_n^*(s)\,ds \end{cases},$$

which is allowed, as $x_n^*(s)$ is strictly monotone in $[T_{4n-1}, T_{4n}]$, we get, using **H2**,

$$c_1 = \frac{k_1}{\gamma_1} \int_{\theta_n - \delta}^{\theta_n + \delta} \frac{\mu_n^{-'}(u)}{2\theta_n - u} du$$

as desired. Similarly for the other coefficients $(c_i)_{i=2,\ldots,n}$ and $(\tilde{c}_i)_{i=1,\ldots,n}$. ∎

Thanks to Lemmas 3.3 and 4.2, we are now in a position to establish our main result, which gives the stability of every periodic orbit of F_μ under **H1**, **H2**, and **H3**.

Theorem 4.3. *Assume the conditions* **H**1, **H**2, *and* **H**3 *are satisfied. Let* $x^*(t)$ *be a periodic orbit of* $\Sigma^\mu_{\theta,k,\gamma,\delta}$ *following cycle* $\mathcal{C}$ *with period* T. *Then* 1 *belongs to the spectrum of the monodromy matrix* $\mathfrak{S}(Z(T))$, *and all other eigenvalues satisfy* $|\lambda| < 1$.

Proof. Under **H**3, it follows that $U(c_1, 0) = U(\tilde{c}_1, 0)$ and $W(c_2, \ldots, c_n, 0) = W(\tilde{c}_2, \ldots, \tilde{c}_n, 0)$, and the monodromy matrix can be written $Z(T_{4n}) = A^2$, where $A = e^{-\gamma T/2} U(c_1, 0) W(c_2, \ldots, c_n, 0)$, which has the form

$$A = e^{-\gamma T/2} \begin{bmatrix} 1 + c_1 c_2 \cdots c_n & c_1 c_3 \cdots c_n & c_1 c_4 \cdots c_n & \cdots & c_1 c_n & c_1 \\ c_2 & 1 & 0 & \cdots & 0 & 0 \\ c_2 c_3 & c_3 & 1 & \cdots & 0 & 0 \\ c_2 c_3 c_4 & c_3 c_4 & c_4 & \cdots & 0 & 0 \\ \vdots & \vdots & \vdots & \vdots & \vdots & \vdots \\ c_2 \cdots c_n & c_3 \cdots c_n & c_4 \cdots c_n & \cdots & c_n & 1 \end{bmatrix}.$$

To compute the characteristic polynomial of A, χ_A, it suffices to do the following operations on the columns $Q_1, \ldots, Q_n$ of A,

$$\forall 1 \le i \le n-1, \ Q_i \leftarrow Q_i - c_{i+1} Q_{i+1}$$
$$Q_n \leftarrow Q_n,$$

and then to develop with respect to the last columns. The characteristic polynomial is

(3) $$\chi_A = ((X - e^{-\gamma T/2})^n - c_1 \cdots c_n e^{-\gamma T/2} X^{n-1}).$$

Defining $G := e^{-\gamma T/2}$ and observing that $X = 0$ cannot be a root of χ_A, this polynomial can also be written as

(4) $$\chi_A = G^n (X/G)^{n-1} \left(\frac{(X/G - 1)^n}{(X/G)^{n-1}} - c_1 c_2 \cdots c_n \right) = G^n (X/G)^{n-1} (f(X) - c_1 c_2 \cdots c_n),$$

where the function f is defined by the relation

(5) $$f(x) = \frac{(x/G - 1)^n}{(x/G)^{n-1}}$$

for x nonzero. By Proposition 3.1, and since the monodromy matrix is given by A^2, we know that either 1 or -1 belongs to the spectrum of A. To analyze the characteristic polynomial, we will separately study its real and complex roots.

First case: Real roots. Observe that the sign of the function $f(x)$ satisfies

$$(6) \qquad x < 0 \Rightarrow \quad f(x) = \frac{(-1)^n \, |-x/G + 1|^n}{(-1)^{n-1} \, |x/G|^{n-1}} < 0$$

$$(7) \qquad x \geq G \Rightarrow \quad f(x) = \frac{|x/G - 1|^n}{|x/G|^{n-1}} \geq 0$$

while in the interval $0 < x < G$, it depends on the parity of n, but this will not be needed to establish our result (note further that $G < 1$). The derivative of the function $f(x)$ is

$$\begin{aligned}
\frac{df}{dx} &= \frac{1}{G} \frac{(x/G - 1)^{n-1} \, (x/G)^{n-2}}{(x/G)^{2(n-1)}} \, (x/G + n - 1) \\
&= \frac{1}{G} \frac{(x/G - 1)^{n-1}}{(x/G)^n} (x/G + n - 1) \\
&= \frac{1}{G}(1 - G/x)^{n-1}(1 + (n-1)(G/x)).
\end{aligned}$$

So it is clear that $df/dx > 0$ for all $x > G$ (since all terms are positive) and similarly $df/dx > 0$ for all $x < -(n-1)G$. Next, consider the expression $f(x) - c_1 c_2 \cdots c_n$.

(1.a) If $c_1 c_2 \cdots c_n > 0$, then using (6), $f(x) - c_1 c_2 \cdots c_n < 0$ for all $x < 0$, which implies that χ_A has no real negative roots. It follows that {the monodromy matrix has $\lambda = 1$ as an eigenvalue}, which yields

$$(8) \qquad c_1 c_2 \cdots c_n = \frac{(1 - G)^n}{G}.$$

Since the derivative of $f(x) - c_1 c_2 \cdots c_n$ is equal to that of $f(x)$, we know that $f(x) - c_1 c_2 \cdots c_n$ is strictly increasing for all $x > G$ and thus for $x > 1$; hence, χ_A has no real roots strictly larger than 1.

(1.b) If $c_1 c_2 \cdots c_n < 0$, then using (7), $f(x) - c_1 c_2 \cdots c_n > 0$ for all $x > G$, which implies that χ_A has no real positive root strictly larger than G. In this case, since we have $G < 1$, it follows that the root given by the monodromy matrix is $\lambda = -1$, which yields

$$(9) \qquad c_1 c_2 \cdots c_n = -\frac{(1 + G)^n}{G}.$$

Now, assumption **H3** gives $-(n-1)G > -1$ so that the derivative of $f(x) - c_1 c_2 \cdots c_n$ is strictly positive for all $x < -1 < -(n-1)G$. As $f(-1) = c_1 c_2 \cdots c_n$, χ_A cannot have any real roots below -1.

Together, points (1.a) and (1.b) show that all real roots have indeed magnitude less than 1.

Second case: Complex roots. Let us take $\lambda = re^{i\alpha}$ a complex (nonreal) root of χ_A. As above, there are two cases to consider for $c_1 c_2 \cdots c_n$: positive or negative: We only describe the case $c_1 c_2 \cdots c_n < 0$ since the case $c_1 c_2 \cdots c_n > 0$ is completely similar.

By expression (9), we have

$$\left(re^{i\alpha} - G\right)^n = e^{i\pi} \, (G + 1)^n \left(re^{i\alpha}\right)^{n-1},$$

and thus there exists an integer $0 \le k \le n$ such that

$$r e^{i\alpha} - G = (G+1)\, r^{\frac{n-1}{n}}\, e^{i\, \frac{(n-1)\alpha+(2k+1)\pi}{n}},$$

which yields:

$$\begin{cases} r\cos\alpha - G &= (G+1)\, r^{\frac{n-1}{n}}\, \cos\frac{(n-1)\alpha+(2k+1)\pi}{n} \\ r\sin\alpha &= (G+1)\, r^{\frac{n-1}{n}}\, \sin\frac{(n-1)\alpha+(2k+1)\pi}{n}. \end{cases}$$

Notice that $\frac{\alpha-(2k+1)\pi}{n} \notin \pi\mathbb{Z}$; otherwise, λ would belong to $\mathbb{R}$. Now we have

$$(r\cos\alpha - G)\sin\alpha = (r\cos\alpha - G)(G+1)\, r^{\frac{-1}{n}}\sin\frac{(n-1)\,\alpha+(2k+1)\,\pi}{n}$$

$$= (G+1)\, r^{\frac{n-1}{n}}\cos\frac{(n-1)\,\alpha+(2k+1)\,\pi}{n}\sin(\alpha),$$

which gives

$$r^{\frac{n-1}{n}}\left(\cos(\alpha)\sin\frac{(n-1)\,\alpha+(2k+1)\,\pi}{n} - \sin(\alpha)\cos\frac{(n-1)\,\alpha+(2k+1)\,\pi}{n}\right)$$

$$= G\, r^{\frac{-1}{n}}\sin\frac{(n-1)\,\alpha+(2k+1)\,\pi}{n}.$$

Using the identity formula $\sin(a-b) = \sin(a)\cos(b) - \sin(b)\cos(a)$, we finally get

$$r = G\,\kappa\,(\alpha),$$

where $\kappa\,(\alpha)$ denotes the function

$$\kappa\,(\alpha) := \frac{\sin\left(\frac{(n-1)\alpha+(2k+1)\pi}{n}\right)}{\sin\left(\frac{-\alpha+(2k+1)\pi}{n}\right)}$$

defined for α such that $\frac{\alpha-(2k+1)\pi}{n} \notin \pi\mathbb{Z}$.

By assumption **H3**, we have $G < \frac{1}{n-1}$; it thus remains to verify that $\kappa(\alpha) < n - 1$ to get that $r = |\lambda| < 1$. To do this, it suffices to observe the relation

$$\frac{(n-1)\,\alpha+(2k+1)\,\pi}{n} = (n-1)\left(\frac{\alpha-(2k+1)\,\pi}{n}\right) + (2k+1)\,\pi,$$

which yields that $\kappa\,(\alpha)$ is of the form

$$\kappa\,(\alpha) = \frac{\sin\left((n-1)\,\omega\right)}{\sin\left(\omega\right)}$$

with $\omega = \frac{\alpha-(2k+1)\pi}{n}$. Applying the identity $|\sin((n-1)\omega)| \le (n-1)|\sin(\omega)|$ (which can be proven by induction in a very straightforward way), we get $\kappa(\alpha) \le n - 1$ and thus

$$r = G\,\kappa\,(\alpha) \le (n-1)\,G < 1$$

as desired.

In the case $c_1 \cdots c_n > 0$, the exact similar reasoning gives

$$r = G \, \tilde{\kappa}\,(\alpha)\,,$$

where $\tilde{\kappa}\,(\alpha)$ denotes this time the function

$$\tilde{\kappa}\,(\alpha) := \frac{\sin\left(\frac{(n-1)\alpha+2k\pi}{n}\right)}{\sin\left(\frac{-\alpha+2k\pi}{n}\right)},$$

and therefore the same inequality $r = G\,\tilde{\kappa}(\alpha) < 1$ holds as well in this case.

In conclusion, if hypotheses **H1**–**H3** are satisfied, then the eigenvalues of $Z(T)$ (other than $\lambda = 1$) satisfy $|\lambda| < 1$. $\blacksquare$

Remark 4.4. Instead of hypothesis **H3**, we could have required a condition only on the parameters c_i as follows.

H3′: $\forall i \in \{1, \ldots, n\} :\; c_i = \tilde{c}_i$ and either $c_1 \cdots c_n < -2^n$ or $c_1 \cdots c_n > (n-1)(\frac{n-2}{n-1})^n$.

This states that the absolute value of $c_1 \cdots c_n$ should be large. In the case $c_1 \cdots c_n > 0$, the inequality is equivalent to $G < 1/(n-1)$ (since in this case $c_1 \cdots c_n = \frac{(1-G)^n}{G}$, as we stated in the proof of Theorem 4.3), while in the case $c_1 \cdots c_n < 0$, the inequality is equivalent to G strictly smaller than a value close to $1/2^n$ (since in this case $c_1 \cdots c_n = \frac{-(1+G)^n}{G}$), a value much smaller than $1/(n-1)$. We thus have **H3′** $\Rightarrow$ **H3**. In fact, **H3** gives the highest upper bound on G that still guarantees existence of an asymptotically stable periodic orbit.

To illustrate Theorem 4.3, let us give an example of vector field F_μ in $\mathbb{R}^3$ satisfying simultaneously the three assumptions **H1**–**H3**. This example can be generalized in a straightforward way to the case $n > 3$.

Example 4.5. Let us define the functions μ_1^+, μ_2^+, and μ_3^- of $\Sigma_{\theta,k,\gamma,\delta}^\mu$ by

$$\mu_i^-(u) = \begin{cases} 1 & \text{if } u \leq \theta_i - \delta \\ 1 - \frac{3}{4\delta^3}[-\left(\theta_i^2 - \delta^2\right)u + \theta_i u^2 - \frac{1}{3}u^3 + \frac{1}{3}\left(\theta_i - \delta\right)^2\left(\theta_i + 2\delta\right)] & \text{if } u \in [\theta_i - \delta, \theta_i + \delta] \\ 0 & \text{if } \theta_i + \delta \leq u \end{cases}$$

and

$$\mu_i^+ = 1 - \mu_i^-, \text{ for } i = \{1, 2, 3\}.$$

The function μ_i with $\theta_i = 9$ and $\delta = 1.5$ is illustrated in Figure 1 (left). Then, with such a definition of F_μ, if assumptions **H1** and **H2** hold, assumption **H3** is true as well. Indeed, we have

$$\forall u \in \{\theta_3 - \delta, \theta_3 + \delta\} :\; {\mu_3^-}'(u) = -\frac{3}{4\delta^3}[(2\theta_3 - u)\,u - \left(\theta_3^2 - \delta^2\right)],$$

which gives, according to Lemma 4.2,

$$c_1 = -\frac{3}{4\delta^3}\frac{k_1}{\gamma_1}\int_{\theta_3-\delta}^{\theta_3+\delta} u\,du + \frac{3}{4\delta^3}\left(\theta_3^2 - \delta^2\right)\frac{k_1}{\gamma_1}\int_{\theta_3-\delta}^{\theta_3+\delta}\frac{1}{2\theta_3 - u}\,du$$

$$= -\frac{3}{4\delta^3}\frac{k_1}{\gamma_1}\int_{\theta_3-\delta}^{\theta_3+\delta}(2\theta_3 - u)\,du + \frac{3}{4\delta^3}\frac{k_1}{\gamma_1}\left(\theta_3^2 - \delta^2\right)\int_{\theta_3-\delta}^{\theta_3+\delta}\frac{1}{u}\,du$$

$$= \tilde{c}_1.$$

By computing the integral terms in c_1, we notice that

$$c_1 = \frac{3}{4\delta^3}\frac{k_1}{\gamma_1}\left(\left(\theta_3^2 - \delta^2\right)\ln\left(\frac{\theta_3 + \delta}{\theta_3 - \delta}\right) - 2\delta\theta_3\right) = \tilde{c}_1.$$

In a completely similar way, we get $c_2 = \tilde{c}_2$, $c_3 = \tilde{c}_3$ and

$$c_2 = \frac{-3}{4\delta^3}\frac{k_2}{\gamma_2}\left(\left(\theta_1^2 - \delta^2\right)\ln\left(\frac{\theta_1 + \delta}{\theta_1 - \delta}\right) - 2\delta\theta_1\right) = \tilde{c}_2$$

$$c_3 = \frac{-3}{4\delta^3}\frac{k_3}{\gamma_3}\left(\left(\theta_2^2 - \delta^2\right)\ln\left(\frac{\theta_2 + \delta}{\theta_2 - \delta}\right) - 2\delta\theta_2\right) = \tilde{c}_3.$$

It remains to verify **H3**. To do this, we make a Taylor expansion of the coefficients above as functions of δ, as δ can be taken as small as desired. We have

$$c_1 = \frac{3}{4\delta^3}\frac{k_1}{\gamma_1}\left(\left(\theta_3^2 - \delta^2\right)\ln\left(1 + \frac{2\delta}{\theta_3 - \delta}\right) - 2\delta\theta_3\right)$$

$$= -2\frac{\theta_1}{\theta_3}\left(1 + \frac{1}{5}\delta^2\right) + o\left(\delta^2\right) \quad \text{as } \delta \to 0$$

and, similarly,

$$c_2 = 2\frac{\theta_2}{\theta_1}\left(1 + \frac{1}{5}\delta^2\right) + o\left(\delta^2\right) \quad \text{as } \delta \to 0$$

$$c_3 = 2\frac{\theta_3}{\theta_1}\left(1 + \frac{1}{5}\delta^2\right) + o\left(\delta^2\right) \quad \text{as } \delta \to 0,$$

which gives $c_1 c_2 c_3 < -2^3$ for $\delta > 0$ small enough. So for $\delta > 0$ small enough, the condition **H3′** (and thus **H3**) is satisfied.

Finally, as a simple consequence of Theorem 4.3, the main result of this paper follows.

Corollary 4.6. *Consider the system $\Sigma_{\theta,k,\gamma,\delta}^{\mu}$, and assume the conditions **H1**, **H2**, and **H3** of Theorem 4.3 are satisfied. Then all the periodic orbits of $\Sigma_{\theta,k,\gamma,\delta}^{\mu}$ following cycle $\mathcal{C}$ are asymptotically stable.*

Proof. Under **H1**, **H2**, and **H3**, Theorem 4.3 ensures that all the eigenvalues of $\Sigma_{\theta,k,\gamma,\delta}^{\mu}$ distinct from 1 have their magnitude smaller than 1. By Property 3.1, this means that all periodic orbits of $\Sigma_{\theta,k,\gamma,\delta}^{\mu}$ following $\mathcal{C}$ are asymptotically stable. ∎

In particular, this corollary establishes that, given any invariant torus contained in cycle $\mathcal{C}$, all fixed points of the return map associated to any Poincaré section of such a torus are asymptotically stable. (Notably, the fixed points in the Poincaré section of the torus in which lies the periodic orbit γ^μ we found in [18] are asymptotically stable.) Now, it is well known from the Lefschetz Fixed-Point Theory (see, for instance, [12, Chapter 3, section 4]) that this implies there exists a unique such fixed point for each such Poincaré return map.

Corollary 4.7. *Consider the system $\Sigma^\mu_{\theta,k,\gamma,\delta}$, and assume the conditions $\boldsymbol{H}1$, $\boldsymbol{H}2$, and $\boldsymbol{H}3$ of Theorem 4.3 are satisfied. Then in each invariant torus contained in cycle $\mathcal{C}$ there exists a unique periodic orbit, which is asymptotically stable.*

5. Explicit expressions for the orbit localization and period. This section illustrates our theoretical results and, in particular, helps to better understand how the symmetry hypotheses H1–H3 play their role in shaping the dynamics of system Σ^μ. Using our results, we will derive an expression for the period of the orbit in terms of the parameters of the system and show that it can be simplified under the symmetries of the system. The accuracy of these approximations will be evaluated by comparison to numerical period values, obtained from randomly generated negative feedback circuits of the form Σ^μ, with either freely chosen parameters or satisfying hypotheses H1–H3. From this numerical analysis, it will become clear that hypotheses H1–H3 imply a pinpointed correspondance between our approximated period formula and numerical computations.

By definition, the period of the orbit is the time it takes the trajectory to complete the first return to a Poincaré section. Alternatively, along cycle $\mathcal{C}$, (and for each coordinate x_i), the period can be divided into two parts: the time it takes variable x_i to first decrease from its maximal to its minimal amplitude and then back. For instance, x_1 strictly increases throughout $B_{0\cdots01} \to B_{0\cdots00} \to \cdots \to B_{2\cdots20}$ and strictly decreases throughout $B_{2\cdots21} \to B_{2\cdots22} \to \cdots \to B_{0\cdots02}$ (since x_1 is repressed by x_n, and x_n is above its threshold in these six boxes). Furthermore, observe that during each of these "half-periods," the expression of $\dot{x}_1$ is *independent* of the other variables.

Therefore, assuming a_i and b_i are, respectively, the minimal and maximal amplitudes of coordinate x_i ($i = 1, \ldots, n$), which satisfy $a_i < \theta_i - \delta < \theta_i + \delta < b_i$, the corresponding increasing or decreasing right-hand side expressions are given by

$$
\begin{aligned}
a_i \rightsquigarrow b_i : & \quad \dot{x}_i = k_i - \gamma_i x_i \\
b_i \rightsquigarrow a_i : & \quad \dot{x}_i = -\gamma_i x_i.
\end{aligned}
$$

Hence, the two "half-periods" can be computed separately and explicitly,

$$
\begin{aligned}
a_i \rightsquigarrow b_i : & \quad T^i_{up} = \frac{1}{\gamma_i} \log \frac{k_i/\gamma_i - a_i}{k_i/\gamma_i - b_i} \\
b_i \rightsquigarrow a_i : & \quad T^i_{dw} = \frac{1}{\gamma_i} \log \frac{b_i}{a_i},
\end{aligned}
$$

yielding the formula $T = T^i_{up} + T^i_{dw}$, where the difficulty lies in calculating a_i and b_i in terms of the parameters k_i, γ_i.
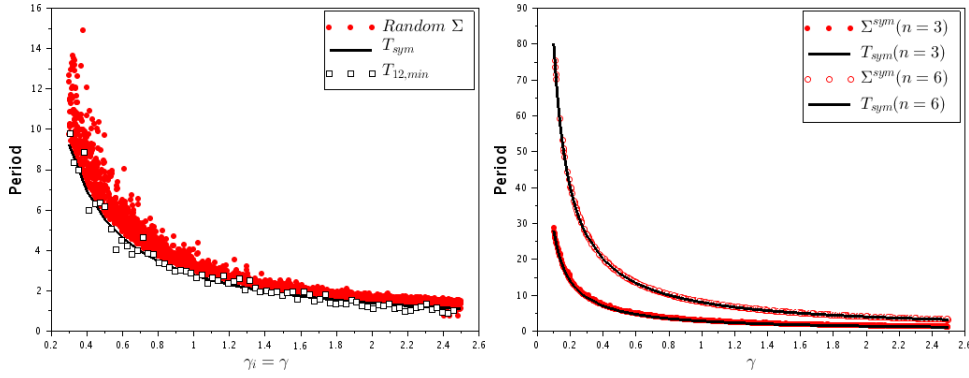
Figure 3. *Numerical period (red dots) for randomly generated Σ^{μ} systems, shown as a function of $\gamma_i = \gamma$. The solid black lines represent the line $T_{sym} = L/\gamma$ with $L = 2\log(2/\alpha - 1)$ and $\alpha = 0.4$ (see text). Left: three-dimensional systems with randomly chosen parameters. The open squares represent the minimal period estimates T_{min}. Right: three- and six-dimensional systems with randomly chosen parameters satisfying symmetry assumptions H1–H3.*

Notice that the set of a_i and b_i, for $i = 1, \ldots, n$, provides the localization of the orbit within the invariant torus. To have an idea of the dependence of a_i, b_i on the system's parameters, we have performed numerical simulations with randomly generated systems Σ^{μ} (as indicated below in Remark 5.2).

5.1. Approximated formulas for localization and period of the orbit (general case).
Numerical simulations with randomly chosen parameters suggest the existence of a *minimum period* in terms of the degradation rates (see the lower limiting curve in Figure 3). In fact, the existence of such a minimal period can be deduced from the equations. First, note that the full period has the form

$$T = \frac{1}{\gamma}\left(\log(r) + \log(r + \varepsilon)\right)$$

for some r and $\varepsilon > 0$. Since $\log(r)$ is a strictly increasing function in $[0, +\infty)$, for each γ, *the minimum value of T is obtained for $\varepsilon \approx 0$*. This means

$$\frac{k_i/\gamma_i - a_i}{k_i/\gamma_i - b_i} = \frac{b_i}{a_i} \quad \Leftrightarrow \quad \left(\frac{b_i}{a_i}\right)^2 - \frac{1}{a_i}\frac{k_i}{\gamma_i}\left(\frac{b_i}{a_i}\right) + \frac{1}{a_i}\frac{k_i}{\gamma_i} - 1 = 0,$$

a quadratic equation which yields either $\frac{b_i}{a_i} = 1$, which is not possible by assumption, or $\frac{b_i}{a_i} = \frac{1}{a_i}\frac{k_i}{\gamma_i} - 1$, which leads to

$$(10) \qquad\qquad\qquad\qquad \frac{k_i}{\gamma_i} = a_i + b_i.$$

In other words, the minimal periods are obtained when the periodic orbit satisfies $a_i + b_i = k_i/\gamma_i$. To go one step further, consider the case of a simple expression for a_i, b_i satisfying (10), such as

$$(11) \qquad\qquad\qquad \tilde{a}_i = \alpha\theta_i, \quad \tilde{b}_i = \frac{k_i}{\gamma_i} - \alpha\theta_i,$$

with $\alpha \in (0, 1)$. In this way, an estimate for the minimal period becomes

$$T_{min} \approx \frac{2}{n} \sum_{i=1}^{n} \frac{1}{\gamma_i} \log \left(\frac{k_i}{\gamma_i} \frac{1}{\alpha \theta_i} - 1 \right).$$

The corresponding values are also shown in Figure 3 and indicate that T_{min} *recovers the functional dependence of the period on the system's parameters*, possibly up to a scaling factor.

Furthermore, expressions (10) and (11) provide an *estimate for the location of the periodic orbit* in terms of the known parameters of the system, k_i, γ_i, and θ_i. This rough estimation suggests that periodic orbits cross the boundaries between regular domains at points satisfying approximately $x_{i-1} = \theta_{i-1}$ and $x_i = \tilde{a}_i$ (going up) or $x_i = \tilde{b}_i$ (going down) (see also Figure 8).

5.2. Localization and period formulas are validated under symmetry hypotheses H1–H3. Our theoretical results are based on three hypotheses that require the system to have several symmetry properties. In fact, these hypotheses allow a simplification of the period formula previously obtained. H1–H2 state that $k_i = 2\theta_i \gamma_i$ and $\gamma_i = \gamma$, so the minimal time T_{min} can be written as

(12)
$$T_{sym} \approx \frac{2}{\gamma} \log \left(\frac{2}{\alpha} - 1 \right),$$

an expression which is *independent of parameters θ_i*. In other words, under the symmetry hypotheses, the period of the negative feedback circuit depends only on the degradation rate and parameter α. This deduction is confirmed by numerical simulations, shown in Figure 3 (right): Indeed, the computed numerical period follows expression T_{sym} very closely.

Furthermore, a striking observation is that *the orbit localization approximation* (11)*is in extremely good agreement with simulations of systems under* H1–H3 (see Figure 4). That is, for each i, the minimal (a_i) and maximal (b_i) amplitudes of the periodic orbit are both effectively linear functions of parameter θ_i. This result is illustrated in Figure 8, for the *Arabidopsis thaliana* model (section 6). The dashed lines in the projection subplots represent $x_i \in \{\alpha \theta_i, k_i/\gamma_i - \alpha \theta_i\}$ (with $\alpha = 0.4$) and $x_{i-1} = \theta_{i-1}$. For instance, in the (x_1, x_2)-plane, it can be seen that the periodic orbit crosses the plane $x_1 = \theta_1$ at $x_2 = \alpha \theta_2$ (as x_1 increases) or $x_2 = (2 - \alpha)\theta_2$ (as x_1 decreases), as predicted by the expressions (11). This is indeed the case for all (x_{i-1}, x_i)-plane projections.

Remark 5.1 (interpretation of parameter α). Parameter α is the slope of the lines in Figure 4, a proportionality constant that depends only on the dimension of the system, and defines a relation between the dimension of a system, its degradation rate, and its period. Consequently, expression G in H3, H3$'$ can be written in term of α as

(13)
$$G_{sym} = e^{-\gamma T_{sym}/2} = \frac{\alpha}{2 - \alpha}.$$

One of the inequalities in hypothesis H3$'$, for the case $c_1 \cdots c_n < 0$, can be writen as

(14)
$$-\frac{(1 + G_{sym})^n}{G_{sym}} < -2^n \quad \Leftrightarrow \quad \alpha(2 - \alpha)^{n-1} < 1.$$
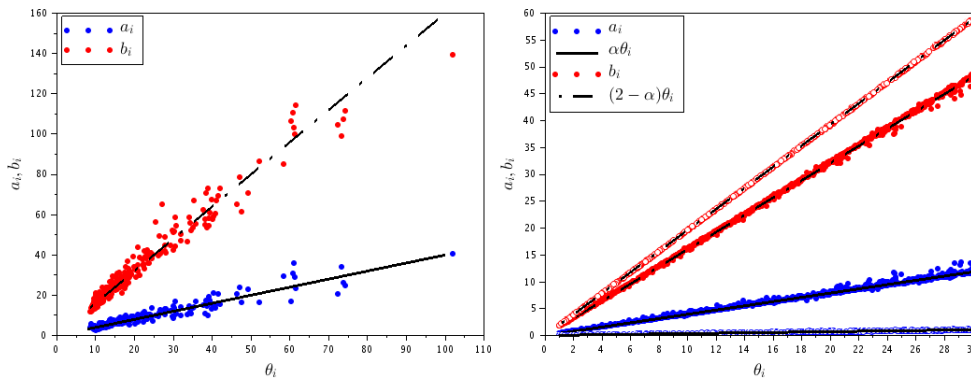
Figure 4. *Numerical values a_i and b_i (blue and red dots) for systems with minimal period as a function of θ_i. The black lines represent, respectively, $\alpha\theta_i$ or $2 - \alpha\theta_i$. Results are shown for randomly chosen systems of dimension 3 (left) and for systems satisfying the symmetry assumptions H1–H3 (right). In the latter case, results are shown for systems of dimension $n = 3$ (blue/red dots) and $n = 6$ (blue/red open circles).*
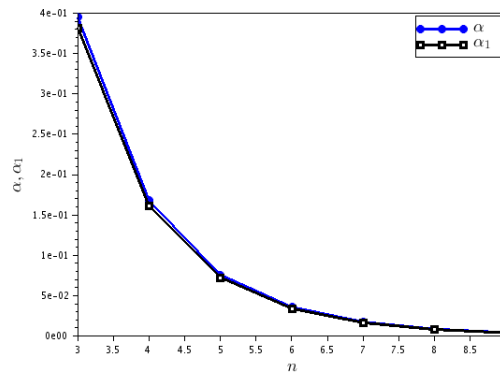

Figure 5. *Comparison of numerical solutions of $\alpha_1(2 - \alpha_1)^{n-1} - 1 = 0$ (black squares) and numerical values of the slope $\alpha \approx a_i/\theta_i$ (blue dots) as a function of the system's dimension, n.*

Now, to further explore the dependence of α on n, consider $\alpha_1(n)$ to be the solution of the *equality*: $\alpha_1(2 - \alpha_1)^{n-1} - 1 = 0$. Numerically solving this equation for each $n \in \{3, \ldots, 9\}$ yields the solutions represented by black squares in Figure 5. The slopes α from Figure 4 are represented as blue dots. From Figure 5, we can conclude that parameter α tends to maximize the period of the system while satisfying the inequality $c_1 \cdots c_n < -2^n$ in hypothesis H3′.

Remark 5.2 (numerical simulations methodology). To randomly generate systems, the parameters were chosen from uniform distributions in the following intervals:

$$\text{General case: } n = 3, \quad k_i \in [30, 60], \quad \gamma \in [0.3, 2.5], \quad \theta_i \in \left[9, 0.7\frac{k_i}{\gamma}\right].$$

$$\text{Symmetric case: } n \in \{3, 4, \ldots, 9\}, \quad \gamma \in [0.1, 2.5], \quad \theta_i \in [1, 30], \quad k_i = 2\gamma\theta_i.$$

In the general case, the functions μ were taken to be nonmonotonic of the form shown in Figure 1 (right). In the symmetric case, the functions μ were of the form given in Example 4.5 and Figure 1 (left). The number of simulations is $N = 500$ for each n. For each simulation, the
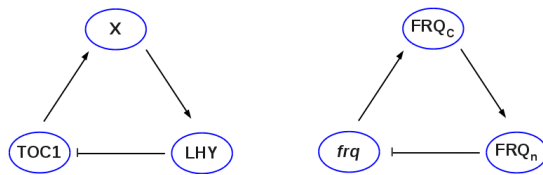
Figure 6. *Negative feedback loops at the basis of circadian rhythms in Arabidopsis thaliana (left) and Neurospora crassa (right).*

period of the periodic orbit is computed numerically, as are the maximum (b_i) and minimum (a_i) amplitudes of each coordinate.

6. Application to biological oscillators: Circadian rhythms. The negative feedback circuit theoretically studied in the previous sections is now used to model two different examples of biological oscillators. As discussed in the introduction, the core of most circadian rhythm mechanisms is composed by such a negative feedback circuit (Figure 6).

To fit the model to the data, we will assume three-dimensional systems Σ^μ satisfying hypotheses H1–H3, according to section 5.2, and estimate the best set of parameters, p^*, that minimize a cost function, defined as follows. Since the data available in both examples extend roughly through a single oscillatory cycle, a cost function was defined to fit essentially the form of the curve rather than the actual data points:

$$J(p^*) = \min_p \left\{ \left| T^{mod}(p) - T^{exp} \right| + \left| a_1^{mod}(p) - a_1^{exp} \right| + \left| b_1^{mod}(p) - b_1^{exp} \right| \right\}.$$

Here, $p = [\theta_1, \theta_2, \theta_3, \gamma, \delta]$ is the set of parameters to estimate; $T^{mod}(p)$, $a_1^{mod}(p)$, and $b_1^{mod}(p)$ are, respectively, the period, the minimal amplitude, and the maximal amplitude of the orbit computed from the numerical model with set of parameters p; and T^{exp}, a_1^{exp}, and b_1^{exp} are the same quantities but measured from the experimental data points.

The fitting results clearly show that, in practice, hypotheses H1–H3 are not really so restrictive as they appear.

6.1. Example 1: Arabidopsis thaliana. The circadian rhythm of the small plant *Arabidopsis thaliana* has been studied in detail. The work of Locke et al. was one of the first to establish the main network of interactions involved in this mechanism [15]. As a first model, Locke et al. proposed a negative feedback circuit where the protein LHY inhibits transcription of $TOC1$ mRNA, which in turn contributes to transcription of LHY mRNA via an intermediate (as yet unidentified) protein X, as illustrated in Figure 6.

In [15], a set of experimental data for $TOC1$ mRNA is given (Figure 5A in that reference). The cost function is defined with the measured quantities

$$T^{exp} = 24h, \quad a_1^{exp} = 0.45, \quad b_1^{exp} = 2.$$

Minimizing the cost function to obtain $J(p^*)$ yields the parameters given in Figure 7. Based on section 5.2, the period for the *Arabidopsis thaliana* three-dimensional ($\alpha = 0.39$) negative loop with $\gamma = 0.12h^{-1}$ is therefore $T_{AT} = \frac{2}{\gamma} \log(2/\alpha - 1) = 23.6h$, which corresponds well to the measured oscillation of the biological system.
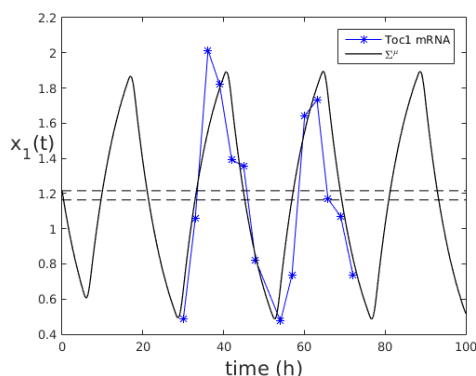
Figure 7. *Fitting Arabidopsis thaliana TOC1 mRNA data* [15] *to a negative feedback circuit* Σ^μ *under hypotheses H1–H3 with μ given by Example* 4.5. *The parameters are $\gamma = 0.12$, $\theta = [1.19, 0.87, 0.21]'$, and $\delta = 0.026$. The period, computed by the formula T_{sym}, is 23.6 hours.*
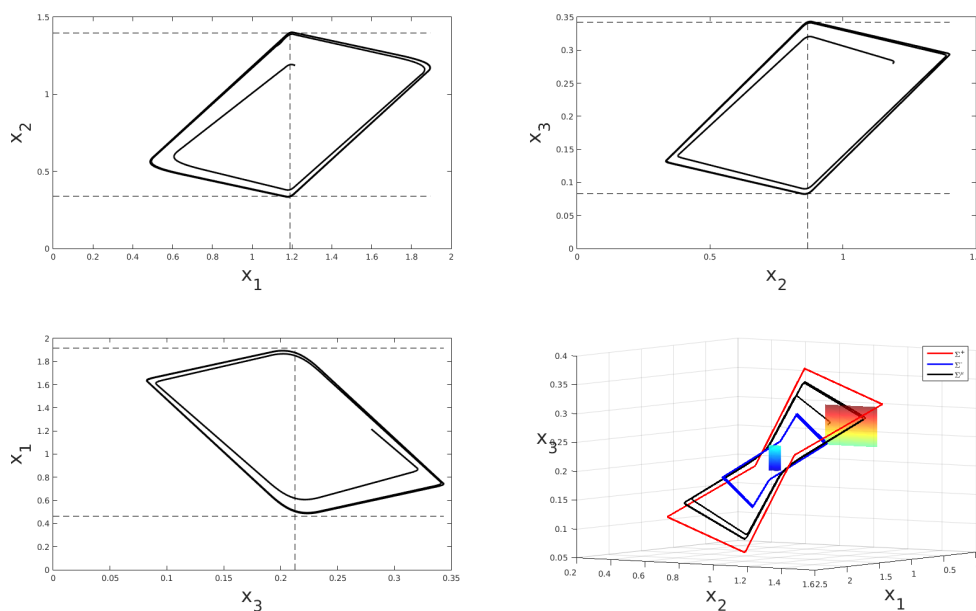

Figure 8. *Dynamics of Arabidopsis thaliana–fitted model. A trajectory starting from the Poincaré section is projected into two-dimensional views, where the dashed lines correspond to $x_{i-1} = \theta_i$ and $x_i = \alpha\theta_i$ or $x_i = (2 - \alpha)\theta_i$ with $\alpha = 0.39$. The corresponding pairs $(i-1, i)$ are $(1, 2)$, $(2, 3)$, and $(3, 1)$. The bottom right subplot represents the three-dimensional trajectory. The periodic orbit (black curve) of system Σ^μ is inside the invariant torus defined by the interior (blue curve) and exterior (red curve) systems. The Poincaré section is shown as a graded green-to-red plane. The middle region containing a fixed point is shown in blue.*

6.2. Example 2: Neurospora crassa. Red bread mold *Neurospora crassa* is another organism exhibiting well-defined circadian rhythms. In [19], a negative feedback circuit involving three elements related to the *frequency (frq)* gene was proposed as a model of its circadian clock: *frq* mRNA (*frq*) contributes to translation of FRQ protein in the cytoplasm (FRQ$_{cyt}$), which is then imported into the nucleus (FRQ$_{nuc}$); finally, in the nucleus, FRQ$_{nuc}$ represses transcription of *frq* (Figure 6).
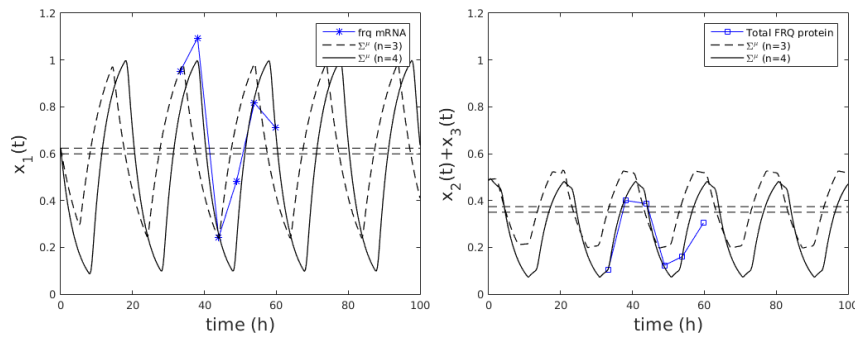
Figure 9. *Fitting Neurospora crassa frq mRNA and FRQ protein data* [19] *to a negative feedback circuit* Σ^μ *of dimension* $n = 3$ *or* $n = 4$, *under hypotheses* H1–H3 *with* μ *given by Example* 4.5. *The parameters are for* $n = 3$, $\gamma = 0.145$, $\theta = [0.61, 0.11, 0.25]'$, *and* $\delta = 0.012$ *and for* $n = 4$, $\gamma = 0.246$, $\theta = [0.55, 0.072, 0.20, 0.07]$, *and* $\delta = 0.012$. *The period, computed by the formula* T_{sym}, *is* 19.6 *hours* ($n = 3$) *or* 19.4 *hours* ($n = 4$). *Several cycles of the model are shown, but there is only one cycle of mRNA and protein measurements (six data points) available in this experiment, given in arbitrary units and scaled to a common quantity.*

Using the experimental data in [19] (Figure 5(a) and 5(b)) for *frq* mRNA and total FRQ protein at 21°C, the measured quantities used in the cost function are

$$T^{exp} = 20h, \quad a_1^{exp} = 0.2, \quad b_1^{exp} = 1, \quad a_{23}^{exp} = 0.1, \quad b_{23}^{exp} = 0.4.$$

Here, a_{23} and b_{23} represent, respectively, the minimum and maximum amplitudes of total FRQ protein, to be compared with the model's $\min(x_2(t) + x_3(t))$ and $\max(x_2(t) + x_3(t))$. It should be remarked that mRNA and protein data are given in arbitrary units, scaled to a common quantity. Since the clock circuit could involve other steps, we have fitted *Neurospora* data to systems Σ^μ of dimensions 3 and 4, with the results shown in Figure 9. Qualitatively, the fit is quite good in both cases, but the model with $n = 4$ appears to be slightly better, suggesting a longer circuit. Based on section 5.2, computation of the period from formula (12) is around 19.5 hours for both models, which corresponds to the period measured from the data.

7. Conclusion. This paper studies a system composed of a negative feedback loop where the regulatory functions have a window of "uncertainty," described by a smooth function, monotonic or not. The existence of an invariant torus in the state space as well as the existence of a periodic orbit within this torus were established in previous work, using comparison to piecewise linear systems.

Here, under some particular assumptions on the symmetry of the system, we have proved that all the periodic orbits of the system $\Sigma^\mu_{\theta,k,\gamma,\delta}$ following cycle $\mathcal{C}$ are asymptotically stable: This has been done thanks to the analysis of the spectra of the monodromy matrices associated with these periodic orbits. From this fact, we can deduce the uniqueness of the periodic orbit inside each invariant torus contained in $\mathcal{C}$. Therefore, our method permits a good tracking of the stable periodic orbits inside the phase space of the class of smooth models considered. This approach could be used for other, similar models with more complicated regulation functions.

However, the stability is not global: Indeed, it is easy to check that, in many cases, the system also admits a steady state in the middle domain ($[\theta_i - \delta, \theta_i + \delta]$). Alternatively, there could be, for instance, two disjoint Poincaré sections inside all of these switching domains,

forming by the way two invariant torii (one of them being the one we found in [18]) in each of which would lie a unique asymptotically stable periodic orbit and, outside these two torii, an unstable periodic orbit following another cycle than $\mathcal{C}$.

An advantage of our comparison approach is the fact that the system is allowed to have a short window with unknown behavior (the length of this window is to be calibrated to each system), as may often happen with biological regulatory functions. An interesting outcome from our analysis is the explicit computation of the period in terms of the parameters. Under the symmetry hypotheses, the period depends only on the degradation rate and the system's dimension through a parameter α which maximizes the period while satisfying the constraints given by the hypotheses (notably H3′). Therefore, if the degradation rates are known, our analysis can provide an indication of the number of necessary elements in the negative feedback loop to reach the observed period, which is helpful for practical biological purposes, namely, for the search of possible intermediate genes. As illustrated by the *Arabidopsis* and *Neurospora* examples, our modeling approach is suitable for analyzing biological oscillatory phenomena, either in the more general form given in [18] or under the symmetry hypotheses we required here.

REFERENCES

[1] V. Arnold, *Ordinary Differential Equations*, Springer-Verlag, Heidelberg, 1992.

[2] D. Bell-Pedersen, V. Cassone, D. Earnest, S. Golden, P. Hardin, T. Thomas, and M. Zoran, *Circadian rhythms from multiple oscillators: Lessons from diverse organisms*, Nat. Rev. Genet., 6 (2005), pp. 544–556.

[3] R. Casey, H. De Jong, and J.-L. Gouzé, *Piecewise-linear models of genetic regulatory networks: Equilibria and their stability*, J. Math. Biol., 52 (2006), pp. 27–56.

[4] M. B. Elowitz and S. Leibler, *A synthetic oscillatory network of transcriptional regulators*, Nature, 403 (2000), pp. 335–338, https://doi.org/10.1038/35002125.

[5] C. Feillet, G. van der Horst, F. Levi, D. Rand, and F. Delaunay, *Coupling between the circadian clock and cell cycle oscillators: Implication for healthy cells and malignant growth*, Front. Neurol., 6 (2015), pp. 1–7.

[6] P. François, N. Despierre, and E. Siggia, *Adaptive temperature compensation in circadian oscillations*, PLoS Comput. Biol., 8 (2012), p. e1002585.

[7] T. Gedeon, *Oscillations in monotone systems with a negative feedback*, SIAM J. Appl. Dyn. Syst., 9 (2010), pp. 84–112.

[8] L. Glass, *Classification of biological networks by their qualitative dynamics*, J. Theor. Biol., 54 (1975), pp. 85–107, https://doi.org/http://dx.doi.org/10.1016/S0022-5193(75)80056-7.

[9] A. Goldbeter, *Biochemical Oscillations and Cellular Rhythms: The Molecular Bases of Periodic and Chaotic Behaviour*, Cambridge University Press, Cambridge, MA, 1996.

[10] B. C. Goodwin, *Oscillatory behavior in enzymatic control processes*, Adv. Enzyme Regulation, 3 (1965), pp. 425–438, http://view.ncbi.nlm.nih.gov/pubmed/5861813.

[11] J. Griffith, *Mathematics of cellular control processes. I. Negative feedback to one gene*, J. Theor. Biol., 20 (1968), pp. 202–208.

[12] V. Guillemin and P. A., *Differential Topology*, Prentice Hall, Englewood Cliffs, NJ, 1974.

[13] J. Hale, *Ordinary Differential Equations*, Wiley-Interscience, New York, 1969.

[14] S. P. Hastings, J. J. Tyson, and D. Webster, *Existence of periodic solutions for negative feedback cellular control systems*, J. Differential Equations, 25 (1977), pp. 39–64.

[15] J. Locke, M. Southern, L. Kozma-Bognar, V. Hibberd, P. Brown, M. Turner, and A. Millar, *Extension of a genetic network model by iterative experimentation and mathematical analysis*, Mol. Syst. Biol., 0013 (2005), pp. 1–9.

[16] J. Mallet-Paret and G. R. Sell, *The Poincaré-Bendixson theorem for monotone cyclic feedback systems with delay*, J. Differential Equations, 125 (1996), pp. 441–489.

[17] J. Mallet-Paret and H. L. Smith, *The Poincaré-Bendixson theorem for monotone cyclic feedback systems*, J. Dyn. Differential Equations, 2 (1990), pp. 367–421, https://doi.org/10.1007/BF01054041.

[18] C. Poignard, M. Chaves, and J.-L. Gouzé, *Periodic oscillations for nonmonotonic smooth negative feedback circuits*, SIAM J. Appl. Dyn. Syst., 15 (2016), pp. 257–286.

[19] P. Ruoff, J. Loros, and J. Dunlap, *The relationship between frq-protein stability and temperature compensation in the Neurospora circadian clock*, Proc. Natl. Acad. Sci., 102 (2005), pp. 17681–17686.

[20] T. Y.-C. Tsai, Y. S. Choi, W. Ma, J. R. Pomerening, C. Tang, and J. E. Ferrell, *Robust, tunable biological oscillations from interlinked positive and negative feedback loops*, Science, 321 (2008), pp. 126–129, http://www.ncbi.nlm.nih.gov/pmc/articles/PMC2728800/.